Journal of Computational Physics **177,** 117–133 (2002)
doi:10.1006/jcph.2002.7006, available online at http://www.idealibrary.com on IDEAL®

A Fully Conservative Second-Order Finite Difference Scheme for Incompressible Flow on Nonuniform Grids

F. E. Ham, F. S. Lien, and A. B. Strong

Department of Mechanical Engineering, University of Waterloo, Waterloo, Ontario, Canada, N2L 3G1
E-mail: feham@sunwise.uwaterloo.ca, fslien@sunwise.uwaterloo.ca,
and astrong@sunwise.uwaterloo.ca

Received March 26, 2001; revised December 7, 2001

A second-order-accurate finite difference discretization of the incompressible Navier–Stokes is presented that discretely conserves mass, momentum, and kinetic energy (in the inviscid limit) in space and time. The method is thus completely free of numerical dissipation and potentially well suited to the direct numerical simulation or large-eddy simulation of turbulent flow. The method uses a staggered arrangement of velocity and pressure on a structured Cartesian grid and retains its discrete conservation properties for both uniform and nonuniform gird spacing. The predicted conservation properties are confirmed by inviscid simulations on both uniform and nonuniform grids. The capability of the method to resolve turbulent flow is demonstrated by repeating the turbulent channel flow simulations of H. Choi and P. Moin (1994, *J. Comput. Phys.* **113**, 1), where the effect of computational time step on the computed turbulence was investigated. The present fully conservative scheme achieved turbulent flow solutions over the entire range of computational time steps investigated ($\Delta t^+ = \Delta t u_\tau^2/\nu = 0.4$ to 5.0). Little variation in statistical turbulence quantities was observed up to $\Delta t^+ = 1.6$. The present results differ significantly from those reported by Choi and Moin, who observed significant discrepancies in the turbulence statistics above $\Delta t^+ = 0.4$ and the complete laminarization of the flow at and above $\Delta t^+ = 1.6$. © 2002 Elsevier Science (USA)

Key Words: Navier–Stokes; DNS; LES; conservation; nonuniform mesh.

1. INTRODUCTION

The direct numerical simulation (DNS) and large-eddy simulation (LES) of turbulent flow require accurate numerical methods to resolve the wide range of spatial and temporal scales inherent to turbulence. Experience has shown that it is not only the order of accuracy

0021-9991/02 $35.00
© 2002 Elsevier Science (USA)
All rights reserved.

of the discrete approximation that determines the overall accuracy of a given method. Of equal or perhaps even greater importance are the discrete conservation properties of the method. Numerical schemes with good discrete conservation properties in terms of mass, momentum, and kinetic energy have been shown to produce superior results when compared to their nonconservative counterparts [2].

In a recent investigation, Morinishi *et al*. [3] analyzed several finite difference schemes for their conservation properties and derived discretely conservative fourth-order schemes for uniform meshes. The schemes were extended to nonuniform meshes by Vasilyev [4], although the simultaneous discrete conservation of mass, momentum, and kinetic energy was not possible. Only schemes that discretely conserved mass and momentum but not kinetic energy or discretely conserved mass and kinetic energy but not momentum could be developed. This was true even for second-order-accurate schemes on nonuniform meshes. Vasilyev identified the source of the nonconservation as the commutation error between the discrete differencing and averaging operators on the nonuniform mesh.

The concept of discrete conservation can be applied to time as well as space. Morinishi *et al*. did not, however, consider discrete conservation in time as an analytical requirement for a proper set of discretization equations. In the analyses of both Morinishi *et al*. and Vasilyev, time advancement was accomplished by a third-order Runge–Kutta time-stepping method. The authors justified the nonconservation by observing that the associated errors appeared to be dissipative and decreased with the cube of the computational time step. The recent work of Perot [5] on two-dimensional unstructured staggered schemes extends the discrete conservation analysis to include time.

The objective of the present work is to develop a second-order-accurate finite difference scheme for structured nonuniform Cartesian meshes that discretely conserve mass, momentum, and kinetic energy in both space and time and then test its suitability for DNS. To our knowledge, this is the first fully conservative scheme for nonuniform meshes reported in the literature; although we thank a reviewer for bringing to our attention the work of Kajishima [6], who already proposed some elements of the scheme.

The rest of the paper is organized as follows. In Section 2, the concepts of differential and discrete conservation are reviewed. In Section 3, the discrete equations for incompressible flow are presented and their conservation properties derived. In Section 4, the predicted conservation properties are confirmed by inviscid simulations on both uniform and nonuniform grids. Section 4 also includes several "thought" experiments that investigate the computed energy spectra for the inviscid simulations and the reversibility of the scheme in the inviscid limit. In Section 5, the method is applied to the DNS of turbulent plane channel flow to investigate the effect of the computational time step on the computed turbulence. Section 6 presents a summary.

2. CONSERVATION PRINCIPLES

Requiring discrete conservation as an additional constraint for a proper set of discretization equations is an effort to enforce a discrete analogue to the fundamental conservation properties of the governing partial differential equations. In this section, the analytic statements of conservation are reviewed for a fully conservative governing equation, and the analogous discrete statements are developed.

2.1. *Differential Conservation*

Consider the following governing equation for the scalar quantity ϕ,

$$\frac{\partial \phi}{\partial t} + \frac{\partial F_j(\phi)}{\partial x_j} = 0, \tag{1}$$

where F_j is commonly called the flux of ϕ, and summation is implied over repeated indices. The form of Eq. (1) has alternately been referred to as the fully conservative form or the strongly conservative form. Its conservation properties can be illustrated by integrating over field V,

$$\int_V \left(\frac{\partial \phi}{\partial t} + \frac{\partial F_j(\phi)}{\partial x_j} \right) dV = 0. \tag{2}$$

Assuming $V \neq V(t)$ and applying Gauss' divergence theorem to the divergence yields

$$\frac{\partial}{\partial t} \int_V \phi \, dV + \int_S F_j(\phi) n_j \, dS = 0, \tag{3}$$

where S is the surface surrounding volume V, and n_j is the outward surface normal. When V is a control volume (CV), Eq. (3) can be seen as a statement of local conservation—a balance between the rate of change of the amount of ϕ inside the CV and the net flux through the boundary. Alternatively, when V is the entire problem domain, Eq. (3) can be seen as a statement of global conservation.

Consider the case when V is a periodic field, free from the potential sources and sinks introduced by boundaries. In this case, the net flux through the boundary is zero, and Eq. (3) can be simplified to

$$\int_V \phi \, dV = constant. \tag{4}$$

Equation (4) simply states that, in the absence of boundaries, the total amount of ϕ is conserved. Now consider the specific case of the Navier–Stokes equations.

For incompressible flow, the governing Navier–Stokes equations can be written as

$$\frac{\partial u_i}{\partial x_i} = 0, \tag{5}$$

$$\frac{\partial u_i}{\partial t} + \frac{\partial u_j u_i}{\partial x_j} + \frac{\partial p}{\partial x_i} - \frac{\partial \tau_{ij}}{\partial x_j} = 0, \tag{6}$$

where u_i is the velocity vector, p is the pressure divided by the constant density, and τ_{ij} is the viscous stress. Here the convective term is reported in divergence form. Written as such, both the mass and momentum equations are fully conservative.

The governing equation for the kinetic energy, $K = u_i u_i/2$, can be developed by taking the vector dot product of the velocity and the momentum equation,

$$u_i \left(\frac{\partial u_i}{\partial t} + \frac{\partial u_j u_i}{\partial x_j} + \frac{\partial p}{\partial x_i} - \frac{\partial \tau_{ij}}{\partial x_j} \right) = 0. \tag{7}$$

Multiply by u_i and consider each of the four resulting terms,

$$(Time) = u_i \frac{\partial u_i}{\partial t}, \tag{8}$$

$$= \frac{\partial u_i u_i/2}{\partial t}, \tag{9}$$

$$(Conv.) = u_i \frac{\partial u_j u_i}{\partial x_j}, \tag{10}$$

$$= \frac{\partial u_j u_i u_i/2}{\partial x_j} + \frac{1}{2} u_i u_i \frac{\partial u_j}{\partial x_j}, \tag{11}$$

$$(Pres.) = u_i \frac{\partial p}{\partial x_i}, \tag{12}$$

$$= \frac{\partial u_i p}{\partial x_i} - p \frac{\partial u_i}{\partial x_i}, \tag{13}$$

$$(Visc.) = -u_i \frac{\partial \tau_{ij}}{\partial x_j}, \tag{14}$$

$$= -\frac{\partial u_j \tau_{ij}}{\partial x_j} + \tau_{ij} \frac{\partial u_i}{\partial x_j}. \tag{15}$$

With the exception of the second part of the viscous term, which represents the kinetic energy dissipation, all terms are either in conservative form or involve the continuity equation, which is identically zero. Thus the kinetic energy equation, in the inviscid limit, is also fully conservative.

It is this inherently conservative nature of mass, momentum, and kinetic energy (in the inviscid limit) at the differential level that motivates our desire to impose discrete analogues on the discretized system.

2.2. *Discrete Conservation*

There are a variety of discretization techniques available for developing discrete approximations to a set of governing partial differential equations such as the Navier–Stokes equations. The finite volume method would seem a logical choice in this case because it is inherently conservative. A conservative finite volume discretization of momentum will not, however, guarantee conservation of kinetic energy. Because the discrete system is already fully defined through the mass and momentum discretizations, discrete conservation of kinetic energy depends implicitly on the discrete operators selected and the order in which they are applied. In the present work we use the finite difference method to develop the discretization equations mainly because of the mathematical tools for discrete conservation analysis that have been developed to date.

Morinishi *et al.* [3] introduced several discrete operators to investigate the conservation properties of various finite difference schemes. By extending the notation of Morinishi to include time, we define the following discrete differencing operator for structured Cartesian

grids with nonuniform spacing:

$$\left.\frac{\delta_1\phi}{\delta_1 x}\right|_{i,j,k,n} \equiv \frac{\phi^n_{i+1/2,j,k} - \phi^n_{i-1/2,j,k}}{x_{i+1/2} - x_{i-1/2}}. \tag{16}$$

In the above definition, ϕ represents a discrete variable and $[i, j, k, n]$ its associated mesh indices in the x, y, z, and t directions respectively (not to be confused with Cartesian tensor indices). Although the stencil size used throughout the present analysis is always 1 (indicated by the "1" subscript), it is retained for consistency with the more general Morinishi definitions. Discrete operators in the y, z (alternatively x_2, x_3), and t directions are similarly defined.

Using this differencing operator, we make the following statement and then endeavor to prove it: A discretization equation discretely conserves the scalar ϕ in space and time when it can be written in the form

$$\frac{\delta_1\phi}{\delta_1 t} + \frac{\delta_1 F_j(\phi)}{\delta_1 x_j} = 0. \tag{17}$$

$F_j(\phi)$ in this case is a discrete approximation for the flux (its exact form is not important here). The discrete conservation properties can be illustrated by considering a number of CVs that together form volume V. Taking the sum of discrete equations multiplied by their respective volume ΔV is the discrete analogue of the integration performed in Eq. (2),

$$\sum_V \left(\frac{\delta_1\phi}{\delta_1 t} + \frac{\delta_1 F_j(\phi)}{\delta_1 x_j}\right)\Delta V = 0. \tag{18}$$

Because the time difference commutes with the summation and all internal fluxes cancel, leaving only those on the surface S, Eq. (18) can be rewritten as

$$\frac{\delta_1}{\delta_1 t}\left(\sum_V \phi\, \Delta V\right) + \sum_S F_j(\phi) n_j \Delta S = 0. \tag{19}$$

Equation (19) is a discrete analogue of Eq. (3) and represents a similar statement of conservation in a discrete sense. Note also that when V is a periodic field, the summation of surface fluxes goes to zero, and Eq. (19) can be simplified to

$$\sum_V \phi^n \Delta V = \sum_V \phi^{n+1} \Delta V = constant, \tag{20}$$

which is a discrete analogue of Eq. (4).

In summary, any discretization equation that can be expressed in the form of Eq. (18) discretely conserves the scalar ϕ in space and time.

3. NUMERICAL METHOD

The numerical method of the present contribution is based on a second-order-accurate discretization of the incompressible Navier–Stokes equations for structured Cartesian meshes with nonuniform spacing and a staggered arrangement of velocity and pressure. In the

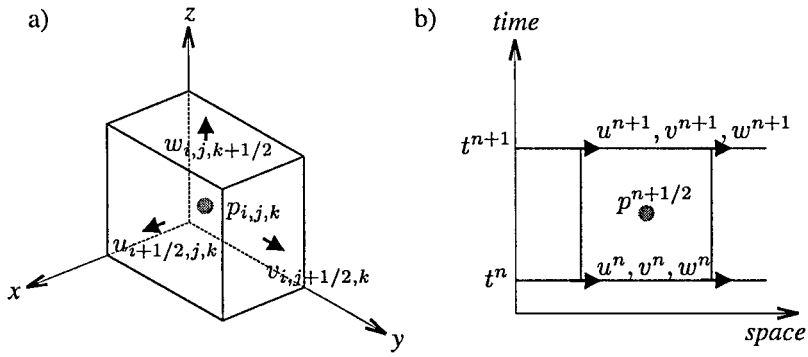

FIG. 1. Staggered variable arrangement in (a) space and (b) space/time.

following subsections, the staggered variable arrangement is described in both space and time, several discrete averaging operators and identities are introduced, the conservative discretization equations are presented and analyzed, and the accuracy of the method is considered. An efficient solution technique for the resulting fully implicit, nonlinear system is also briefly described.

3.1. *Staggered Variable Arrangement*

The staggered arrangement of velocity and pressure, originally by Harlow and Welch [7], has the advantage of ensuring strong coupling between velocity and pressure without requiring special interpolation techniques. Staggering also appears necessary to produce discrete methods with good conservation properties, and as such it forms the basis of the present scheme.

On the staggered grid, pressure p is stored at the CV centers and denoted by the integer subscripts $[i, j, k]$. The Cartesian velocity components u, v, and w are stored at the center of the east, north, and top CV faces respectively. Their staggered location relative to the CV center is denoted by an appropriate half-index shift, as shown in Fig. 1a.

Vasilyev points out that, on nonuniform meshes, the locations of the velocity and pressure points are somewhat ambiguous; they can be determined as the geometric volume and face centers in either physical or computational space. In the present work we choose physical space and define the mesh in terms of the face locations. For example, the west face of the CV at $[i, j, k]$ is at $x_{i-1/2}$, and the east face at $x_{i+1/2}$. The x location of the cell center can then be calculated as the simple average of the adjacent face coordinates,

$$x_i = \frac{1}{2}\left(x_{i-1/2} + x_{i+1/2}\right). \tag{21}$$

The y and z directions are handled similarly.

Because the present work also considers conservation in time, we append the superscript n to all discrete variables to denote their time levels. Figure 1b illustrates how the velocity and pressure locations are also staggered in time. We adopt the convention that the new velocity values in any time step are at time level t_{n+1} and the previous values at t_n. Pressure is then located at the midpoint between these time levels, $t_{n+1/2}$.

3.2. *Additional Discrete Operators and Identities*

In addition to the discrete differencing operator defined by Eq. (16), the following averaging operators will be required to develop and analyze the conservative discretization:

$$\bar{\phi}^{1x}|_{i,j,k,n} \equiv \frac{\phi^n_{i+1/2,j,k} + \phi^n_{i-1/2,j,k}}{2}, \tag{22}$$

$$\widetilde{\phi\psi}^{1x}|_{i,j,k,n} \equiv \frac{1}{2}\left(\phi^n_{i+1/2,j,k}\psi^n_{i-1/2,j,k} + \phi^n_{i-1/2,j,k}\psi^n_{i+1/2,j,k}\right). \tag{23}$$

In the above definitions, ϕ and ψ represent discrete variables tha may be cell-centered or staggered, and $[i, j, k, n]$ are the associated indices in the x, y, z, and t directions respectively. Discrete operators in the y, z, and t directions are similarly defined.

Unfortunately, kinetic energy conservation does not appear to be possible on nonuniform grids when only these operators are used to discretize the incompressible Navier–Stokes equations. As pointed out by Vasilyev [4], the violation in conservation is related to the commutation error between the discrete differencing and averaging operators,

$$\frac{\delta_1\bar{\phi}^{1x}}{\delta_1 x} \neq \overline{\frac{\delta_1\phi}{\delta_1 x}}^{1x}. \tag{24}$$

This inequality can be verified by expanding both sides using the operator definitions. Expanding the left-hand side at the cell-center location $[i, j, k, n]$ yields

$$\begin{aligned}\left.\frac{\delta_1\bar{\phi}^{1x}}{\delta_1 x}\right|_{i,j,k,n} &= \frac{[\bar{\phi}^{1x}]_{i+1/2,j,k,n} - [\bar{\phi}^{1x}]_{i-1/2,j,k,n}}{x_{i+1/2} - x_{i-1/2}} \\ &= \frac{1}{2}\left(\frac{\phi^n_{i+1,j,k} - \phi^n_{i-1,j,k}}{x_{i+1/2} - x_{i-1/2}}\right).\end{aligned}$$

Expanding the right-hand side at the same location yields

$$\begin{aligned}\left.\overline{\frac{\delta_1\phi}{\delta_1 x}}^{1x}\right|_{i,j,k,n} &= \frac{1}{2}\left(\left[\frac{\delta_1\phi}{\delta_1 x}\right]_{i+1/2,j,k,n} + \left[\frac{\delta_1\phi}{\delta_1 x}\right]_{i-1/2,j,k,n}\right) \\ &= \frac{1}{2}\left(\frac{\phi^n_{i+1,j,k} - \phi^n_{i,j,k}}{x_{i+1} - x_i} + \frac{\phi^n_{i,j,k} - \phi^n_{i-1,j,k}}{x_i - x_{i-1}}\right) \\ &= \left(\frac{\phi^n_{i+1,j,k} - \phi^n_{i,j,k}}{x_{i+3/2} - x_{i-1/2}} + \frac{\phi^n_{i,j,k} - \phi^n_{i-1,j,k}}{x_{i+1/2} - x_{i-3/2}}\right).\end{aligned}$$

Here Eq. (21) has been used to express the denominators in terms of the staggered grid locations. Clearly the operators do not commute. Nor do they commute when expanded about the staggered location $[i + 1/2, j, k, n]$.

To produce conservative schemes on nonuniform meshes, it is necessary to introduce the following weighted averaging operators:

$$\bar{\phi}^{1\bar{x}}|_{i,j,k,n} \equiv \frac{\left(x_i - x_{i-1/2}\right)\phi^n_{i+1/2,j,k} + \left(x_{i+1/2} - x_i\right)\phi^n_{i-1/2,j,k}}{x_{i+1/2} - x_{i-1/2}}, \tag{25}$$

$$\bar{\phi}^{1\bar{x}}|_{i,j,k,n} \equiv \frac{\left(x_{i+1/2} - x_i\right)\phi^n_{i+1/2,j,k} + \left(x_i - x_{i-1/2}\right)\phi^n_{i-1/2,j,k}}{x_{i+1/2} - x_{i-1/2}}. \tag{26}$$

Note that, on uniform meshes, both of these averaging operators reduce to the simple averaging operator of Eq. (22). Also note that, when evaluated at the cell-center locations, both of these averaging operators are the same as the simple averaging operator of Eq. (22), even on nonuniform meshes. This is a result of our definition of cell centers as the geometric center between face locations in physical space, Eq. (21). When evaluated at the staggered locations, however, these two operators have quite different interpretations. Equation (25) is simply the standard linear interpolation. In Eq. (26) the weights are reversed, and it can be thought of as a volume-weighted average. Both averaging operators will be required in the following discrete analysis because commutation with the discrete differencing operator depends on the grid location at which the operator is evaluated. When evaluated at a cell-center location, Eq. (25) commutes with differencing,

$$\left[\frac{\delta_1 \bar{\phi}^{1\hat{x}}}{\delta_1 x} = \frac{\overline{\delta_1 \phi}^{1\hat{x}}}{\delta_1 x} = \frac{\overline{\delta_1 \phi}^{1x}}{\delta_1 x} \right]_{x\text{-centered}}, \tag{27}$$

where ϕ in this case represents a variable or expression with a cell-centered x location. When evaluatd at a staggered location, Eq. (26) commutes with differencing,

$$\left[\frac{\delta_1 \bar{\psi}^{1x}}{\delta_1 x} = \frac{\delta_1 \bar{\psi}^{1\bar{x}}}{\delta_1 x} = \frac{\overline{\delta_1 \psi}^{1\bar{x}}}{\delta_1 x} \right]_{x\text{-staggered}}, \tag{28}$$

where ψ represents a variable or expression with a staggered x location. In both Eqs. (27) and (28) the equivalency between the simple average and the weighted average at cell-centered locations has been included where appropriate.

The following identities will also be required to derive some relationships later in the paper. These are nonuniform versions of some of the uniform grid identities presented by Morinishi [3]. First, two discrete operators in different directions always commute. Note that one of the "directions" may be time; for example,

$$\frac{\overline{\delta_1 \phi}^{1x}}{\delta_1 t} = \frac{\delta_1 \bar{\phi}^{1x}}{\delta_1 t}. \tag{29}$$

Second, when evaluated at a cell-centered x location,

$$\left[\overline{\psi \frac{\delta_1 \phi}{\delta_1 x}}^{1\hat{x}} = \frac{\delta_1 \psi \, \bar{\phi}^{1\hat{x}}}{\delta_1 x} - \phi \frac{\delta_1 \psi}{\delta_1 x} \right]_{x\text{-centered}}, \tag{30}$$

where ϕ represents a variable or expression with a cell-centered x location, and ψ is a variable or expression with a staggered x location.

Finally, when evaluated at a staggered location,

$$\left[\psi \frac{\delta_1 \phi \, \bar{\psi}^{1x}}{\delta_1 x} = \frac{1}{2} \frac{\delta_1 \phi \, \widetilde{\psi \psi}^{1x}}{\delta_1 x} + \frac{1}{2} \psi \psi \frac{\delta_1 \phi}{\delta_1 x} \right]_{x\text{-staggered}}, \tag{31}$$

where once again ϕ and ψ represent cell-centered and staggered expressions respectively.

3.3. *Discretization Equations*

Using the discrete operators defined previously, the discretized Navier–Stokes equations are now presented. At this point, it is convenient to return to Cartesian tensor notation. The continuity equation is evaluated at the cell-centered location $[i, j, k, n+1]$ using the following discretization:

$$\frac{\delta_1 u_i}{\delta_1 x_i} = 0. \tag{32}$$

The x, y, and z components of the momentum equation are evaluated at the staggered locations $[i+1/2, j, k, n+1/2]$, $[i, j+1/2, k, n+1/2]$, and $[i, j, k+1/2, n+1/2]$ respectively using the following discretization:

$$\frac{\delta_1 u_i}{\delta_1 t} + \frac{\delta_1 \overline{\overline{u_j}^{1t}}^{1\breve{x}_i} \overline{\overline{u_i}^{1t}}^{1x_j}}{\delta_1 x_j} + \frac{\delta_1 p}{\delta_1 x_i} - \frac{\delta_1 \tau_{ij}}{\delta_1 x_j} = 0, \tag{33}$$

$$\tau_{ij} = \bar{\nu}\left(\frac{\delta_1 \overline{u_i}^{1t}}{\delta_1 x_j} + \frac{\delta_1 \overline{u_j}^{1t}}{\delta_1 x_i}\right), \tag{34}$$

$$\bar{\nu} = \begin{cases} \nu & \text{for } i = j, \\ \overline{\bar{\nu}^{1x_i}}^{1x_j} & \text{for } i \neq j. \end{cases} \tag{35}$$

Note that x_i appearing as a superscript does not follow the summation convention. Clearly both the mass and momentum equations are in the discrete form of Eq. (19), and thus the scheme will discretely conserve mass and momentum in space and time.

As pointed out by Morinishi, local kinetic energy cannot be defined unambiguously on the staggered grid because the velocity components are stored at different locations. The kinetic energy norm conserved by the present system requires the discrete kinetic energy equation to be developed about the mesh location $[i, j, k, n+1/2]$. The vector dot product of the velocity with the momentum equation (33) produces the kinetic energy equation which, including the appropriate discrete second-order interpolations, takes the form

$$\overline{\overline{u_i}^{1t}\left(\frac{\delta_1 u_i}{\delta_1 t} + \frac{\delta_1 \overline{\overline{u_j}^{1t}}^{1\breve{x}_i} \overline{\overline{u_i}^{1t}}^{1x_j}}{\delta_1 x_j} + \frac{\delta_1 p}{\delta_1 x_i}\right)}^{1x_i} = 0. \tag{36}$$

Note that the viscous terms have been omitted. Expanding Eq. (36), we can rearrange each of the three resulting terms as follows. The time term can be rewritten using the operator definitions and Eq. (29) as

$$(Time) = \overline{\overline{u_i}^{1t} \frac{\delta_1 u_i}{\delta_1 t}}^{1x_i}, \tag{37}$$

$$= \overline{\frac{\delta_1 u_i u_i/2}{\delta_1 t}}^{1x_i}, \tag{38}$$

$$= \frac{\delta_1 \overline{u_i u_i/2}^{1x_i}}{\delta_1 t}. \tag{39}$$

The convective term can be rewritten using Eqs. (31), (27), (28), and (29) as

$$(Conv.) = \overline{\overline{u_i}^{1t}\frac{\delta_1\overline{\overline{u_j}^{1t}}^{1\breve{x}_i}\overline{\overline{u_i}^{1t}}^{1x_j}}{\delta_1 x_j}}^{1x_i}, \tag{40}$$

$$= \frac{1}{2}\overline{\frac{\delta_1\overline{\overline{u_j}^{1t}}^{1\breve{x}_i}\widetilde{\overline{u_i}^{1t}\overline{u_i}^{1t}}^{1x_j}}{\delta_1 x_j}}^{1x_i} + \frac{1}{2}\overline{\overline{u_i}^{1t}\overline{u_i}^{1t}\frac{\delta_1\overline{\overline{u_j}^{1t}}^{1\breve{x}_i}}{\delta_1 x_j}}^{1x_i}, \tag{41}$$

$$= \frac{1}{2}\overline{\frac{\delta_1\overline{\overline{u_j}^{1t}}^{1\breve{x}_i}\widetilde{\overline{u_i}^{1t}\overline{u_i}^{1t}}^{1x_j}}{\delta_1 x_j}}^{1\widehat{x}_i} + \frac{1}{2}\overline{\overline{u_i}^{1t}\overline{u_i}^{1t}\frac{\overline{\overline{\delta_1 u_j}^{1t}}^{1\breve{x}_i}}{\delta_1 x_j}}^{1x_i}. \tag{42}$$

The pressure term can be rewritten using Eqs. (30) and (29) as

$$(Pres.) = \overline{\overline{u_i}^{1t}\frac{\delta_1 p}{\delta_1 x_i}}^{1x_i}, \tag{43}$$

$$= \frac{\delta_1\overline{u_i}^{1t}\,\bar{p}^{1\widehat{x}_i}}{\delta_1 x_i} - p\frac{\delta_1\overline{u_i}^{1t}}{\delta_1 x_i}, \tag{44}$$

$$= \frac{\delta_1\overline{u_i}^{1t}\,\bar{p}^{1\widehat{x}_i}}{\delta_1 x_i} - p\frac{\overline{\delta_1 u_i}^{1t}}{\delta_1 x_i}. \tag{45}$$

Because the discrete continuity equation is identically zero, the kinetic energy equation also takes the discrete form of Eq. (17), and thus the scheme discretely conserves kinetic energy (in the inviscid limit) in space and time. The conserved norm can be taken from the time term,

$$K = \overline{u_i u_i/2}^{1x_i}, \tag{46}$$

evaluated at the cell-centered location $[i, j, k, n]$ or $[i, j, k, n+1]$.

To summarize, two key elements are required to produce this fully conservative, second-order-accurate discretization for nonuniform meshes: (1) the convective term must use the product of the average (midpoint) velocities between the two time levels (this has already been pointed out by Perot [5]) and (2) to avoid any commutation error with differencing on the nonuniform mesh, the advecting velocity in the convective term must be interpolated using a volume-weighted average rather than a simple or linear average.

3.4. *Accuracy*

Some discussion of the order of accuracy of the scheme is required, as only one of the three averaging operators, Eq. (25), is formally second-order accurate. The least accurate averaging operator is Eq. (26)—the volume average—where the truncation error can be expressed in terms of the local grid spacing Δx and grid expansion ratio α as

$$\bar{\phi}^{1\breve{x}} = \phi + \frac{1}{2}\frac{\partial\phi}{\partial x}(\alpha - 1)\Delta x + O(\Delta x^2). \tag{47}$$

On uniform grids, $\alpha = 1$, and formal second-order accuracy is recovered. For arbitrary nonuniform grids, however, the accuracy of the interpolation appears to drop to first order.

On grids suitable for DNS and LES, however, the grid spacing is generally not arbitrary. The nonuniform spacing is usually the result of some mapping function $f(\eta)$ where f is continuous and smooth and increases monotonically over the range $0 \le \eta \le 1$:

$$x_i = f(i/N) \qquad i = 0, 1 \ldots N. \tag{48}$$

The Taylor series expansion of f about some $\eta = i/N$ can be used to develop an expression for an adjacent x value,

$$x_{i+1} = f(i/N) + \frac{\partial f}{\partial \eta}\frac{1}{N} + \frac{1}{2}\frac{\partial^2 f}{\partial \eta^2}\frac{1}{N^2} + O\left(\frac{1}{N^3}\right). \tag{49}$$

The difference between Eqs. (48) and (49) yields an approximation for the local grid spacing:

$$\Delta x \approx \frac{\partial f}{\partial \eta}\frac{1}{N}. \tag{50}$$

The expansion ratio α, defined as the ratio between adjacent grid spacings, can also be approximated using the Taylor series,

$$\alpha = \frac{x_{i+1} - x_i}{x_i - x_{i-1}}, \tag{51}$$

$$= \frac{\frac{\partial f}{\partial \eta}\frac{1}{N} + \frac{1}{2}\frac{\partial^2 f}{\partial \eta^2}\frac{1}{N^2} + O\left(\frac{1}{N^3}\right)}{\frac{\partial f}{\partial \eta}\frac{1}{N} - \frac{1}{2}\frac{\partial^2 f}{\partial \eta^2}\frac{1}{N^2} + O\left(\frac{1}{N^3}\right)}, \tag{52}$$

$$\approx 1 + \frac{\frac{\partial^2 f}{\partial \eta^2}}{\frac{\partial f}{\partial \eta}}\frac{1}{N}, \tag{53}$$

which can be rewritten in terms of Δx using Eq. (50):

$$\alpha \approx 1 + \frac{\frac{\partial^2 f}{\partial \eta^2}}{\left(\frac{\partial f}{\partial \eta}\right)^2}\Delta x. \tag{54}$$

When Eq. (54) is substituted into Eq. (47) it is clear that second-order accuracy is recovered for the case of nonuniform grid spacing where the grid distribution is based on a smoothly varying mapping function.

3.5. *Solution Procedure*

The fully implicit, nonlinear system of equations resulting from this choice of discretization can be quite stiff, particularly on the highly stretched grids typical of LES and DNS of wall-bounded shear flows. In the present work, the system is solved iteratively at each time step using Newton linearization and an algebraic multigrid with smoothing based on the symmetric coupled Gauss–Siedel method of Vanka [8]. The system's stiffness is handled by coarsening preferentially in the direction of greatest coefficient strength, a multigrid technique referred to as semicoarsening [9]. With the judicious selection of coarse grids, it is possible to reduce the maximum residual by 6 orders of magnitude with about 50 workunits per time step (where 1 workunit is equivalent to one smoothing sweep

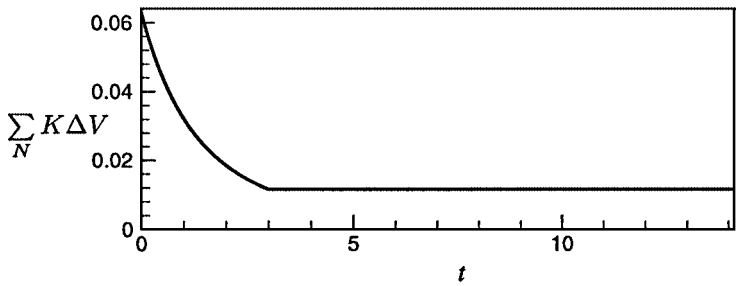

FIG. 2. Time history of total kinetic energy for a 64^3 periodic box simulation. Initial viscosity $\nu = 1/2000$ was set to zero at $t = 3$.

through the finest grid). Although relatively expensive per time step when compared to other DNS/LES solution methods, the present fully implicit system is numerically stable for any choice of computational time step, and the discrete conservation properties ensure that the method is free from numerical dissipation.

4. SIMULATIONS IN A PERIODIC BOX

To test the predicted conservation properties of the method, we carried out inviscid simulations in $1 \times 1 \times 1$ periodic boxes with both uniform and nonuniform grid spacing. The simulations were initialized with a random solenoidal velocity field and integrated ahead in time with finite viscosity. At some point the viscosity was set to zero and the equations were integrated further ahead in time, monitoring the total momentum and kinetic energy. On both the uniform and the nonuniform grids, both quantities were conserved to machine accuracy, confirming the predicted conservation properties of the method.

4.1. *Energy Spectra*

Figure 2 plots the time history of the total kinetic energy for one simulation carried out on a 64^3 uniform grid. During the initial viscous part of the simulation ($0 < t < 3$), the total kinetic energy is seen to decay rapidly due to viscous dissipation. Figure 3a shows the

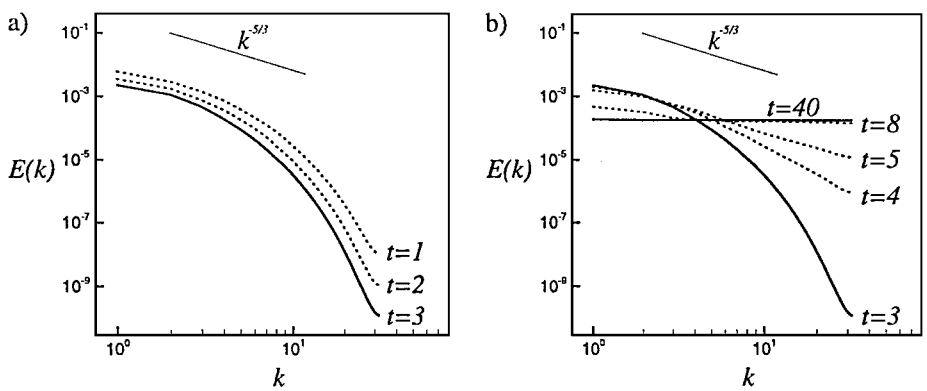

FIG. 3. Computed spatial energy spectra from a 64^3 periodic box simulation. Times refer to Fig. 2. (a) Initial viscous part of the simulation, (b) inviscid part of the simulation illustrating the eventual equidistribution of energy among the wave numbers.

spatial energy spectra calculated at times $t = 1$, 2, and 3. The spectra show strong drop off and little or no energy pileup at the highest wave numbers.

At $t = 3$ the viscosity was set to zero. As Fig. 2 shows, the kinetic energy remains precisely constant thereafter. It is interesting to note how the energy redistributes itself in wave space in the absence of viscosity. Figure 3b shows the spatial energy spectra calculated at times $t = 3$, 4, 5, 8, and 40. The immediate loss of viscous dissipation causes the energy at the highest wave numbers to increase rapidly. The net energy transfer is out of the lowest wave numbers. Eventually, the distribution stabilizes at a point where the energy is equally distributed in wave space—a condition of maximum entropy for this isolated numerical system!

4.2. *Reversibility*

One of the interesting characteristics of the present fully conservative scheme is its reversibility in the inviscid limit. To investigate this reversibility, an inviscid, periodic box simulation was restarted from a saved file and solved with a negative computational time step. No modification to the solution algorithm was required to step backward in time. Figure 4a shows the time history of the x velocity component at one point in the periodic box during the forward-time simulation, leading up to the writing of the restart file at $t = 35$. Figure 4b compares the velocity at the same point calculated by the reverse-time simulation. The reverse-time velocity appears qualitatively identical to the forward-time velocity until about $t = 28$, when the two traces start to differ noticeably.

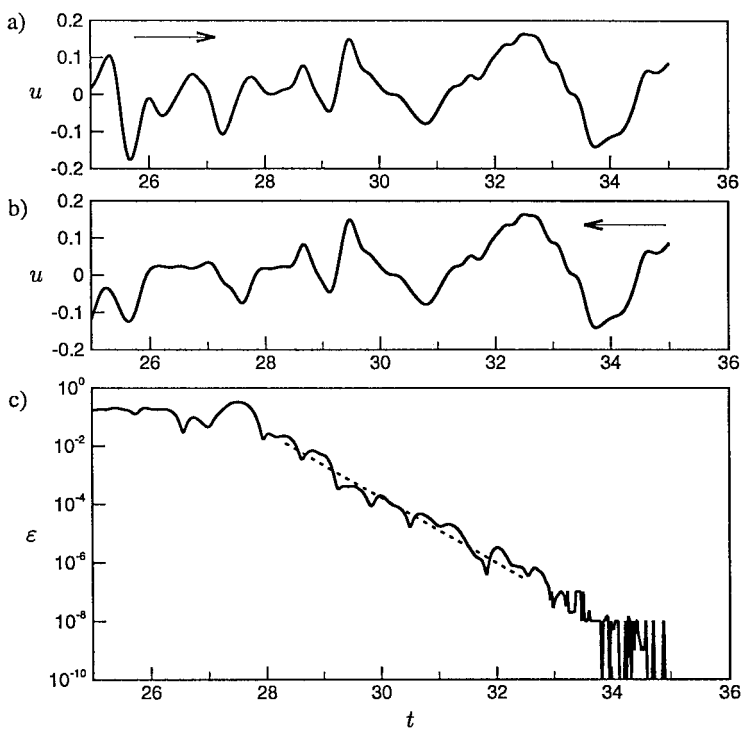

FIG. 4. (a) Time trace of velocity at one point in the inviscid periodic box simulation, (b) veocity calculated at the same point by time-reverse simulation, (c) difference: $\varepsilon = \sqrt{\Delta u^2 + \Delta v^2 + \Delta w^2}$.

A quantitative comparison of the difference in calculated velocities at one point, plotted as Fig. 4c, shows that the eventual departure of the two traces resuts from a relatively steady amplification of errors. For all inviscid simulations in which reversibility was investigated (which included several 64^3 simulations with different total kinetic energies, computational time step sizes, and convergence criteria) the error amplification could be consistently characterized as

$$\varepsilon = \varepsilon_0 e^{\frac{c\sqrt{K}}{\Delta}t}, \tag{55}$$

where Δ is the mesh spacing and the constant c is approximately 0.34.

5. DNS OF PLANE CHANNEL FLOW

The first rigorous investigation of the effect of computational time step on the DNS of turbulent flow was performed relatively recently by Choi and Moin [1]. They used a fully implicit scheme to conclude that the optimal computational time step for the DNS of turbulent channel flow, expressed in wall units, was about $\Delta t^+ = \Delta t u_\tau^2/\nu = 0.4$. For time steps larger than 0.4, their numerical experiments showed the calculated turbulence statistics to vary significantly from their time-step-independent values. Furthermore, they observed the turbulence to completely decay to a laminar state for time steps of $\Delta t^+ = 1.6$ or greater. In conclusion, they suggested the following physical explanation for their observations: "Turbulence fluctuations can only be sustained if the computational time step is appreciably less than the Kolmogorov time scale." They estimated the Kolmogorov time scale in the sublayer to be about 2.4 wall units.

Using the fully conservative finite difference method of the present work, we repeated the identical investigation. Following Choi and Moin, the channel domain and grid distribution was taken from the *minimum flow unit* of Jiminez and Moin [10], with dimensions $\pi\delta \times 2\delta \times 0.289\pi\delta$ in the streamwise, wall-normal, and spanwise directions respectively. The mesh size (in terms of cells) was $16 \times 128 \times 32$, with uniform spacing in both the streamwise and spanwise directions, and a hyperbolic tangent distribution in the wall-normal direction, as described by [10]. All computations were performed at a Reynolds number based on bulk velocity $Re_b = U_b\delta/\nu = 2800$, which corresponded to a Reynolds number based on wall shear velocity of $Re_\tau = u_\tau\delta/\nu \approx 190$.

Figure 5 compares the first part of the time history of the plane-averaged wall shear rates for three different computational time steps. In this case, all simulations started from the

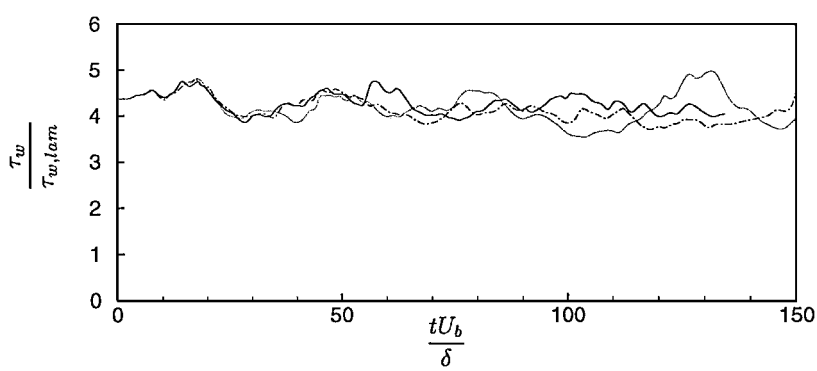

FIG. 5. First part of the time history of plane-averaged wall shear rates for three different computational time steps, all started from the same initial condition: ——— $\Delta t^+ = 0.4$; · · · · · · · $\Delta t^+ = 0.8$; —·—. $\Delta t^+ = 1.2$.

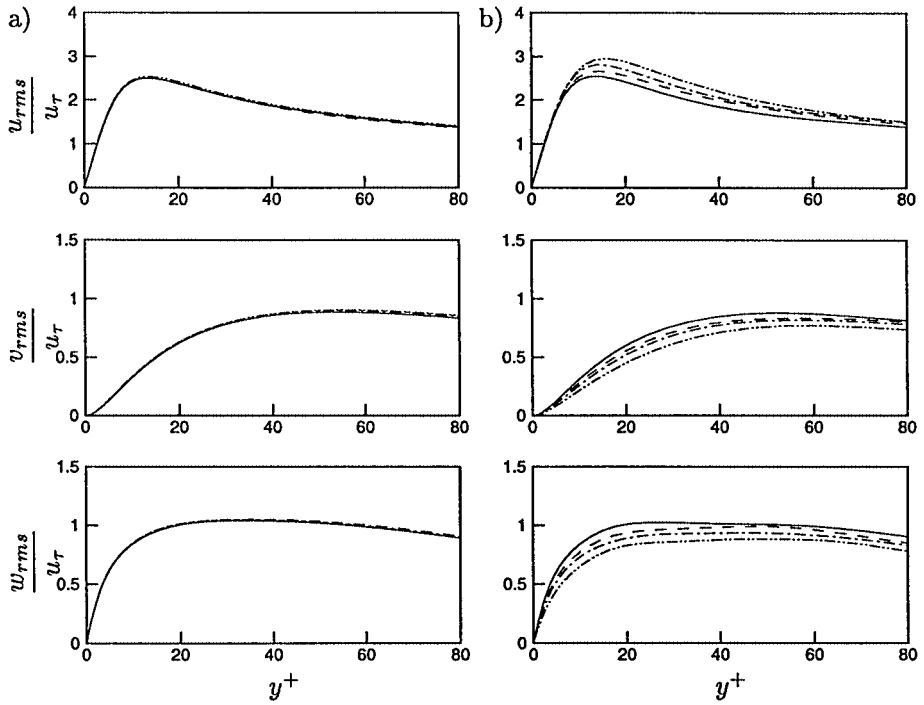

FIG. 6. Variation of root-mean-square velocity fluctuations with the computational time step for (a) present fully conservative scheme and (b) fractional step scheme with present convective discretization: ——— $\Delta t^+ = 0.4$; - - - - $\Delta t^+ = 0.8$; — · —. $\Delta t^+ = 1.2$; — · · — $\Delta t^+ = 1.6$.

same initial condition—a fully developed turbulent flow from a previous simulation. All three simulations exhibited quasi-periodic behavior of the wall shear stress, although the three solutions quickly became uncorrelated.

Figure 6a compares the calculated rms velocity fluctuations for four of the time steps investigated: $\Delta t^+ = 0.4$, 0.8, 1.2, and 1.6. In terms of CFL number, these computation time steps correspond approximately to CFL $= \max(|u_i|/\Delta x_i) = 1$, 2, 3, and 4. We note that these seemingly high CFL numbers are due mainly to the turbulence velocity fluctuations and the relatively fine near-wall grid spacing in the wall-normal direction. Figure 7 compares the Reynolds shear stress for the same four computational time steps. The total averaging time for these simulations was about $600U_b/\delta$.

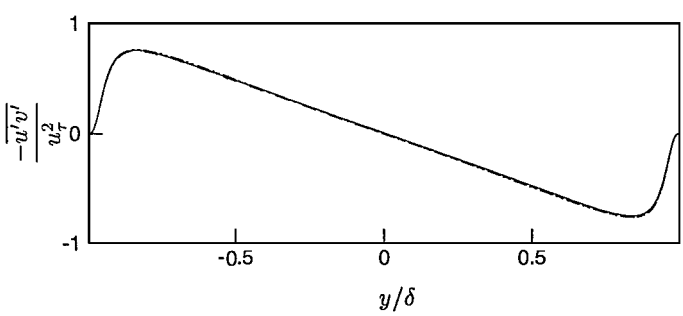

FIG. 7. Variation of Reynolds shear stress with the computational time step for fully conservative scheme: ——— $\Delta t^+ = 0.4$; - - - - $\Delta t^+ = 0.8$; — · — $\Delta t^+ = 1.2$; — · · — $\Delta t^+ = 1.6$.

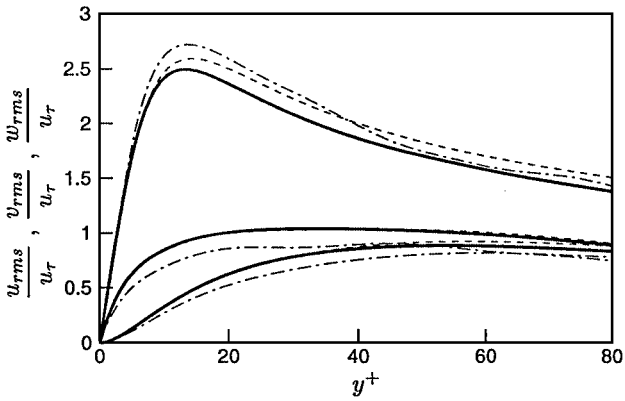

FIG. 8. Variation of root-mean-square velocity fluctuations with the computational time step for very large time steps: ——— time-step-independent result; - - - - $\Delta t^+ = 3.2$; — · —. $\Delta t^+ = 5.0$.

The observed variation in statistical turbulence quantities is significantly smaller than that reported by Choi and Moin, suggesting that their observations may have been a result of dissipative numerical errors associated with their scheme. To clarify whether the source of these errors is related to the difference in the discretization of the convective term (they used Crank–Nicholson) or to the splitting error caused by the fractional step method, several additional simulations were run. These additional simulations used their fractional-step time advancement scheme, but with the convective discretization developed in this paper. Plotted as Fig. 6b, these results show a similar (although slightly reduced) time step sensitivity to that observed by Choi and Moin, suggesting that the splitting error is primarily responsible for the numerical error at large computational time steps. The difference in the convective discretization appears to be a secondary effect, although apparently not an insignificant one. For example, it was possible to get a turbulent solution for $\Delta t^+ = 1.6$, a time step at which Choi and Moin observed the laminarization of the flow.

5.1. *Maximum Computational Time Step*

It remained to determine how much the computational time step could be increased and still appear to resolve the turbulence. To investigate this, several additional turbulent plane channel simulations were performed at computational time steps greater than $\Delta t^+ = 1.6$. Figure 8 compares the computed rms velocity fluctuations for $\Delta t^+ = 3.2$ and 5.0 to the time-step-independent result reported earlier. These time steps correspond to CFL ≈ 8 and 12 respectively.

At $\Delta t^+ = 3.2$ the error in rms velocity fluctuations in the streamwise direction was significant, although the spanwise and wall-normal quantities remained very near their time-step-independent values. At $\Delta t^+ = 5.0$ it did not appear possible to achieve smooth statistical results, and all components contained significant errors. Additionally, at these very large time steps the smoothing sweeps had to be relaxed significantly to ensure convergence, thus negating any potential computational advantage gained by the increased time step.

6. SUMMARY

A second-order-accurate finite difference discretization of the incompressible Navier–Stokes was presented that discretely conserves mass, momentum, and kinetic energy (in the

inviscid limit) in both space and time. The method uses a staggered arrangement of velocity and pressure on a structured Cartesian grid and retains its discrete conservation properties for both uniform and nonuniform grid spacing. The predicted conservation properties were confirmed by inviscid simulations on both uniform and nonuniform grids. The capability of the method to resolve turbulent flow was demonstrated by repeating the turbulent channel flow simulations of Choi and Moin [1], where the effect of computational time step on the computed turbulence was investigated. With the present fully conservative scheme, turbulent flow solutions were achieved over the entire range of computational time steps investigated ($\Delta t^+ = \Delta t u_\tau^2/\nu = 0.4$ to 5.0). Little variation in statistical turbulence quantities was observed up to $\Delta t^+ = 1.6$, corresponding to CFL $= 4$. The present results differ significantly from those reported by Choi and Moin, suggesting that the cause of their observed sensitivity to computational time step may have been the splitting errors associated with their fractional-step time advancement scheme, rather than the more physical explanation they proposed.

ACKNOWLEDGMENT

The authors are grateful to the Natural Sciences and Engineering Research Council of Canada for the financial support of this work. The authors also wish to acknowledge the referees for their helpful comments, which led to the improvement of this manuscript.

REFERENCES

1. H. Choi and P. Moin, Effects of the Computational Time Step on Numerical Solutions of Turbulent Flow, *J. Comput. Phys.* **113**, 1 (1994).
2. R. Mittal and P. Moin, Suitability of upwind-biased finite difference schemes for large-eddy simulation of turbulent flows. *AIAA J.* **35**(8), 1415 (1997).
3. Y. Morinishi, T. S. Lund, O. V. Vasilyev, and P. Moin, Fully conservative higher order finite difference schemes for incompressible flow, *J. Comput. Phys.* **143**, 90 (1998).
4. O. Vasilyev, High order finite difference schemes on non-uniform meshes with good conservation properties, *J. Comput. Phys.* **157**, 746 (2000).
5. B. Perot, Conservation properties of unstructured staggered mesh schemes, *J. Comput. Phys.* **159**, 58 (2000).
6. T. Kajishima, Finite difference method for convective terms using non-uniform grid, *Trans. JSME* **65-633**, 1607 (1999) (in Japanese).
7. F. H. Harlow and J. E. Welch, Numerical calculation of time-dependent viscous incompressible flow of fluid with free surfaces, *Phys. Fluids* **8**, 2182 (1965).
8. S. P. Vanka, A calculation procedure for three-dimensional steady recirculating flows using multigrid methods, *Comp. Meth. Appl. Mech. Eng.* **55**, 321 (1986).
9. P. Wesseling, *An Introduction to Multigrid Methods* (Wiley, New York, 1991).
10. J. Jimenez and P. Moin, The minimal flow unit in near-wall turbulence, *J. Fluid Mech.* **225**, 213 (1991).